The crystal structure of anthranilate phosphoribosyltransferase from the enterobacterium *Pectobacterium carotovorum*

Choel Kim[a], Nguyen-Huu Xuong[a], Steven Edwards[b], Madhusudan[a], Muh-Ching Yee[c], Glen Spraggon[d,*], Stanley E. Mills[e]

[a] *Department of Chemistry/Biochemistry, University of California, San Diego, La Jolla, CA 92093, USA*
[b] *Department of Chemistry and Biochemistry, University of Colorado at Boulder, Campus Box 215, Boulder, CO 80309, USA*
[c] *Department of Biological Sciences, Stanford University, Stanford, CA 94305-5020, USA*
[d] *Genomics Institute of the Novartis Research Foundation, 10675 John Jay Hopkins Drive, La Jolla, CA 92121-1115, USA*
[e] *Department of Biology, University of California, San Diego, La Jolla, CA 92093, USA*

Received 7 May 2002; revised 27 May 2002; accepted 27 May 2002

First published online 25 June 2002

Edited by Hans Eklund

Abstract The structure of anthranilate phosphoribosyltransferase from the enterobacterium *Pectobacterium carotovorum* has been solved at 2.4 Å in complex with Mn^{2+}-pyrophosphate, and at 1.9 Å without ligands. The enzyme structure has a novel phosphoribosyltransferase (PRT) fold and displays close homology to the structures of pyrimidine nucleoside phosphorylases. The enzyme is a homodimer with a monomer of 345 residues. Each monomer consists of two subdomains, α and α/β, which form a cleft containing the active site. The nature of the active site is inferred from the trapped MnPPi complex and detailed knowledge of the active sites of nucleoside phosphorylases. With the anthranilate (An)PRT structure solved, the structures of all the enzymes required for tryptophan biosynthesis are now known. © 2002 Published by Elsevier Science B.V. on behalf of the Federation of European Biochemical Societies.

Key words: Crystal structure; Tryptophan biosynthesis; Anthranilate phosphoribosyltransferase; Pyrimidine nucleoside phosphorylase

1. Introduction

Phosphoribosyltransferases (PRTs) catalyze the Mg^{2+}-dependent group transfer of 5′-phosphoribose from α-D-5-phosphoribosyl-1-pyrophosphate (PRPP) to the nitrogen atom of NH_3 as well as various aromatic heterocyclic and benzene-derived nucleophiles [1]. The enzymes are essential components of nucleotide salvage as well as of the biosynthetic pathways for purines, pyrimidines, niacin, and the amino acids histidine and tryptophan. Shared structural elements among the PRTs have led to their grouping into two classes [2]. Type 1, characterized by a common α/β fold, the PRPP motif, contains all but one of the solved enzyme structures. Quinolinic acid PRT, the single member of Type 2 [3,4], has an N-terminal α/β two-layer sandwich domain, and a C-terminal α/β (TIM) barrel domain.

Anthranilate phosphoribosyltransferase (AnPRT) catalyzes the third of seven reactions leading to L-tryptophan biosynthesis (Scheme 1) [5]. The AnPRT of *Pectobacterium carotovorum* is a homodimer with the monomer consisting of 345 amino acids. Many of the enzyme's properties have been described [6]. In this report we present our initial studies with two crystal forms of AnPRT, one of the apoenzyme, at 1.9 Å, and the other of the protein trapped with PPi and two Mn^{2+} ions, at 2.4 Å. The structure is homologous to those of pyrimidine nucleoside phosphorylase (PYNP, pdb code 1BRW) [7] and thymidine phosphorylase (TP, pdb code 2TPT) [8,9], thereby constituting a third type of PRT fold. With the trapped MnPPi complex as a reference, and structures of the nucleoside phosphorylases as models, it was possible to identify many residues involved in substrate binding.

2. Materials and methods

2.1. Cloning and sequencing of trpD (the gene specifying AnPRT) from P. carotovorum

Genomic DNA isolated from *P. carotovorum* was purified using a CsCl gradient. The isolated DNA was partially digested with *Sau*3A and fragments of 3–4 kb were gel-purified and ligated to dephosphorylated *Bam*HI-cut pUC13. The ligated DNA was transformed into strain JMB9 r^-m^+·*trpLDl02 leu*$^-$ *thr*$^-$ and plated on minimal agar supplemented with 0.05% acid casein hydrolysate, 0.2% glucose, 10 μg/ml anthranilate, 20 μg/ml leucine, 1 μg/ml thiamine and 100 μg/ml ampicillin. Five anthranilate-responding colonies were isolated and analyzed; each had the same 3 kb insert. The sequence was determined by dideoxy sequencing (GenBank accession number AY064465). The insert contained the 3′ half of *trpE*, all of *trpG* and *trpD*, and the 5′ portion of *trpC*. The *trpD* gene was amplified by polymerase chain reaction (PCR) using primers corresponding to −25 nucleotides before the start codon and the end of the cloned insert. This PCR fragment was cloned into a derivative of the expression plasmid ptacterm [10] and the resulting plasmid named pttErD. In this plasmid, expression of *trpD* is under control of the IPTG-inducible *tac* promoter. pttErD was transformed into strain W3110 *metB trpR*·*trpED24* containing pMS421, a plasmid with the $lacI^q$ gene.

2.2. Large scale protein expression, crystallization and data collection

Cells were inoculated into minimal medium plus 0.05% acid casein hydrolysate, 0.2% glucose, 20 μg/ml L-tryptophan, 30 μg/ml L-methionine, 50 μg/ml spectinomycin, 100 μg/ml ampicillin, and grown at 37°C until mid-log phase. IPTG (0.1 M, filter-sterilized) was then added to a final concentration of 1 mM. Cultures were shaken for 4 h at 37°C before harvesting. Cells were disrupted by sonication for protein isolation. The purification procedure has been described [6]. Two crystal forms of AnPRT were obtained by hanging drop vapor diffusion at room temperature. Both crystal forms were grown under the same conditions. The sample was dialyzed against 10 mM HEPES (pH 6.5), 10% glycerol, 1 mM dithiothreitol, 1 mM EDTA and concentrated to 20 mg/ml. A 10 μl aliquot of protein was mixed with an

*Corresponding author. Fax: (1)-858-812 1746.
E-mail address: spraggon@gnf.org (G. Spraggon).

0014-5793/02/$22.00
PII: S0014-5793(02)02905-8

equal volume of 25% polyethylene glycol 3000, 0.2 M HEPES (pH 6.5), 4.5 mM glutamine, 10.0 mM $MnCl_2$, 1.25 mM PRPP, 1.2 μM anthranilate, 1 mM dithiothreitol and 1 mM EDTA. After equilibration, seed crystals were introduced which grew to full size in about 4 days.

All data sets were collected at the UCSD X-ray facility using a unique brilliance Rigaku FR rotating anode X-ray generator under low temperature conditions (approximately −100 K). The MnPPi crystal belongs to space group $P2_12_12$, $a=77.5$ Å, $b=81.5$ Å, $c=102$ Å and diffracted to a minimum Bragg spacing of 2.4 Å resolution. Mercury phenol and samarium nitrate were used as derivatives. Crystals were soaked in solutions of mother liquor containing 50 mM samarium nitrate for 18 h and 20 mM mercury phenol for 24 h. The apoenzyme crystal belongs to space group $P2_12_12_1$, $a=76.9$ Å, $b=82.3$ Å, $c=200$ Å and diffracted to a resolution of 1.9 Å. All data were reduced using DENZO package [11]. Data and phasing statistics are summarized in Table 1.

2.3. Structure solution and refinement

2.3.1. MnPPi crystal. Initial phases for the MnPPi crystal were generated by isomorphous replacement. The substructures of the two derivatives were determined using SHELX [12] and heavy atom positions were refined and experimental phases generated with MLPHARE [13]. Solvent content analysis predicted the asymmetric unit to contain two monomers. Non-crystallographic symmetry operators were found using a self-rotation function and ENVDER [14]. Phases were refined with DM [15] using two-fold non-crystallographic symmetry averaging, solvent flattening and histogram matching. The model was built and refined with Xtalview [16] and CNS [17] using the higher resolution mercury derivative data set. Non-crystallographic symmetry restraints, geometric/temperature factor weights, and temperature factor correlation restraints were evaluated by the behavior of the free *R*-factor set (10% of reflections excluded from the refinement) on application of different refinement strategies. The final *R*-factor and free *R*-factor converged at 21.25% and 26.43% respectively with all residues in allowed regions of the Ramachandran plot. A total of 22 of 345 amino acid residues in each monomer were missing, residues 1–11, 123–132, and 345. The coordinates have been deposited at the Protein Data Bank (code 1KGZ).

2.3.2. Apoenzyme crystal. Initial phases for the apoenzyme crystal were generated with molecular replacement in CNS [17] using the monomer model of the MnPPi crystal as a probe. As in the MnPPi crystal, residues 1–11, 123–132, and 345 were not visible in the electron density. In addition, electron density for residues 94–97 was missing in two of the four subunits. The dimer orientation of the apoenzyme crystal was similar to that of the MnPPi crystal. The structure was both manually and automatically rebuilt using Xtalview [16] and WARP [18]. Water molecules were built with the solvent building mode of WARP [18]. The model was of good geometry with a final *R*-factor of 22.16%. Refinement statistics are summarized in Table 1. The coordinates have been deposited at the Protein Data Bank (code 1KHD).

3. Results and discussion

3.1. General structure

The monomer of AnPRT consists of two subdomains, α and α/β. The α subdomain is a small four-helix bundle, H1–H4, sandwiched next to two additional helices, H8 and H9 (Fig. 2A). The α/β subdomain consists of eight α-helices (H5–H7, H10–H14), one mixed β-sheet with five parallel β-strands (B1–B5), and two anti-parallel β-strands (B6–B7) (Fig. 2A). A Dali [19] search with a partially refined model of the MnPPi bound crystal form revealed AnPRT to be structurally homologous to PYNP [7] and TP [8,9] (Figs. 1 and 4A,B). The α subdomain of AnPRT has a root mean square deviation (rmsd) with PYNP of 1.9 Å on 90 aligned Cα atoms. The α/β subdomain of AnPRT has a rmsd with PYNP of 1.7 Å on 102 aligned Cα atoms. The same subdomain of AnPRT has a rmsd with TP of 1.6 Å on 105 aligned Cα atoms. Relative to AnPRT, PYNP has an additional subdomain containing seven β-strands forming two anti-parallel β-sheets and three extra helices sandwiched in the middle at

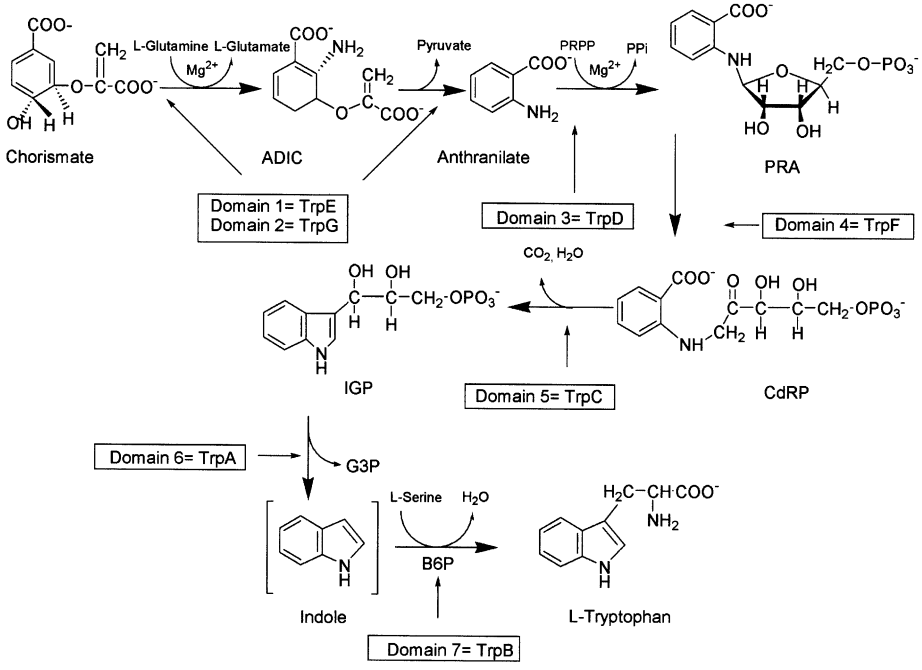

Scheme 1. L-Tryptophan biosynthesis. TrpE, anthranilate synthase; TrpG, glutamine amidotransferase; TrpD, anthranilate phosphoribosyltransferase; TrpF, phosphoribosyl anthranilate isomerase; TrpC, indoleglycerol phosphate synthase; TrpA, indoleglycerol phosphate aldolase; TrpB, L-serine hydro-lyase (adding indole); $TrpE_2TrpG_2$, anthranilate synthase complex; $TrpA_2TrpB_2$, tryptophan synthase complex; ADIC, 2-amino-2′-deoxy-isochorismate; PRPP, 5′-phosphoribosyl-1′-pyrophosphate; PRA, *N*-(5′-phosphoribosyl)-anthranilate; CdRP, 1-(*o*-carboxyphenylamino)-1-deoxyribulose-5-phosphate; B6P, pyridoxal phosphate.

Table 1
Data statistics for *P. carotovorum* AnPRT

Data set	Native		Derivative	
	MnPPi crystal	Apoenzyme crystal	Mercury phenol	Samarium nitrate
Space group	$P2_12_12$	$P2_12_12_1$	$P2_12_12$	$P2_12_12$
Resolution (Å)	50.0–2.44	50.0–1.860	50.0–2.4	50–2.59
No. unique reflections (completeness %)	20457 (98.7%)	99609 (92%)	25162 (98.6%)	20510 (99%)
Average redundancy	3.6	25	5.9	7.7
R_{sym}[a] (%) (highest resolution shell %)	6.7 (39.8)	6.3 (37.2)	7.8 (31.1)	11.3 (53.1)
Number of sites			2	4
Phasing power[b]			1.70	1.72
Figure of merit			0.47	
No. of protein atoms	4936	9691		
No. of hetero atoms	48	0		
No. of waters	201	963		
$R_{crystal}$ (%)	21.25	22.11		
R_{free} (%)	26.43	26.33		
Rmsd bonds (Å)	0.0065	0.0057		
Rmsd angles	1.2	1.2		
Rmsd dihedrals	21.7	21.3		
Rmsd impropers	0.80	0.79		
Mean *B*-factor	45.5	31.5		

[a] $\Sigma_{hkl}\Sigma_i|I_i-\langle I\rangle|/(\Sigma_{hkl}\Sigma_i I_i)$.
[b] Phasing power = $\langle|FH(calc)|\rangle/\langle E\rangle$.

the carboxy terminus [7] (Figs. 1 and 4A). The binding of the substrates in AnPRT occurs within the cleft formed between the two subdomains of the monomer (Figs. 2A,B and 3A,B).

The monomers of AnPRT homodimer are related to each other by a molecular two-fold axis of symmetry (Fig. 2B). The dimer interface is similar to that of PYNP [7] and TP [8,9]. It is confined to the α subdomain, and consists of H1 (residues 13–21), H3 (residues 45–57) and a loop (residues 180–183) between H7 and H8 (Figs. 1 and 2B). Using CNS [17] with a probe radius of 1.4 Å, the surface area occluded upon binding was calculated to be 1700 Å^2.

3.2. Subdomain movement

The asymmetric unit of the apoenzyme crystal contains four

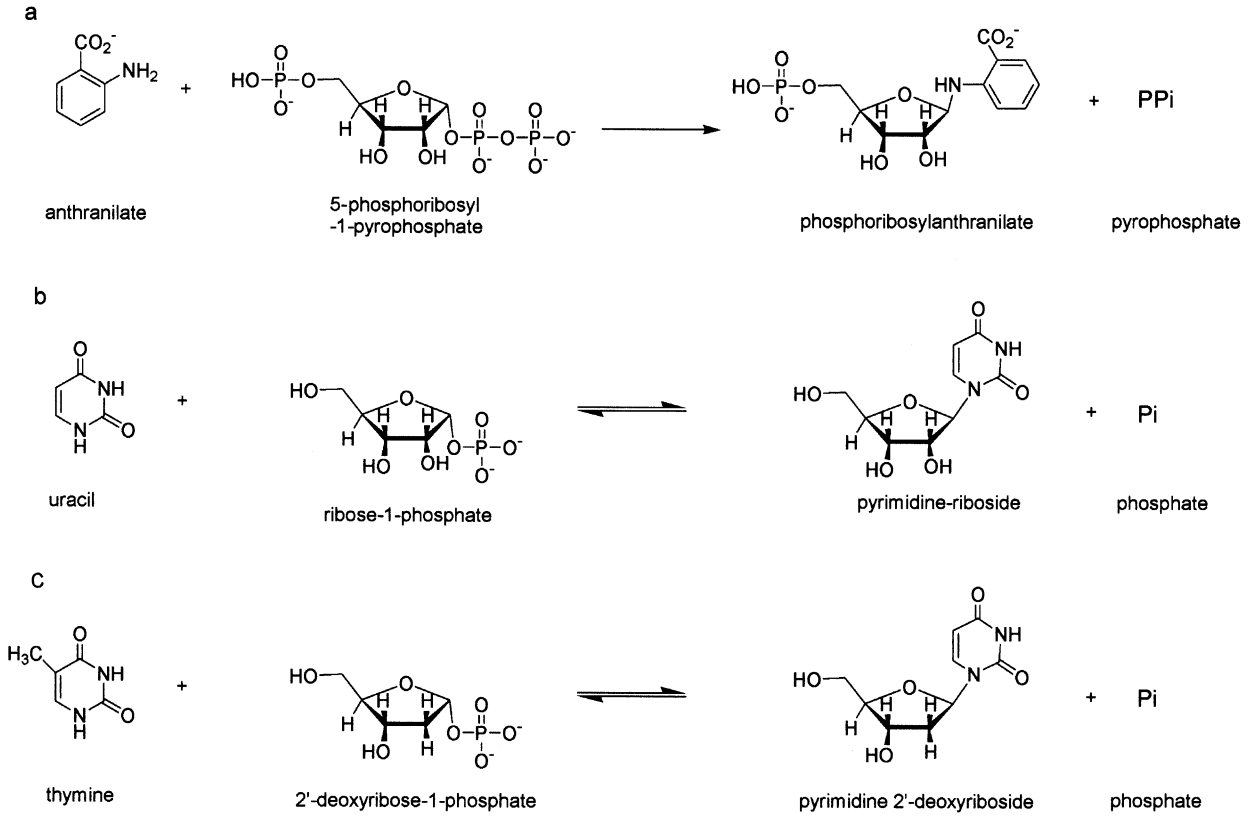

Scheme 2. a: The reaction catalyzed by anthranilate phosphoribosyltransferase. b: The reaction catalyzed by pyrimidine nucleoside phosphorylase. c: The reaction catalyzed by thymidine phosphorylase.

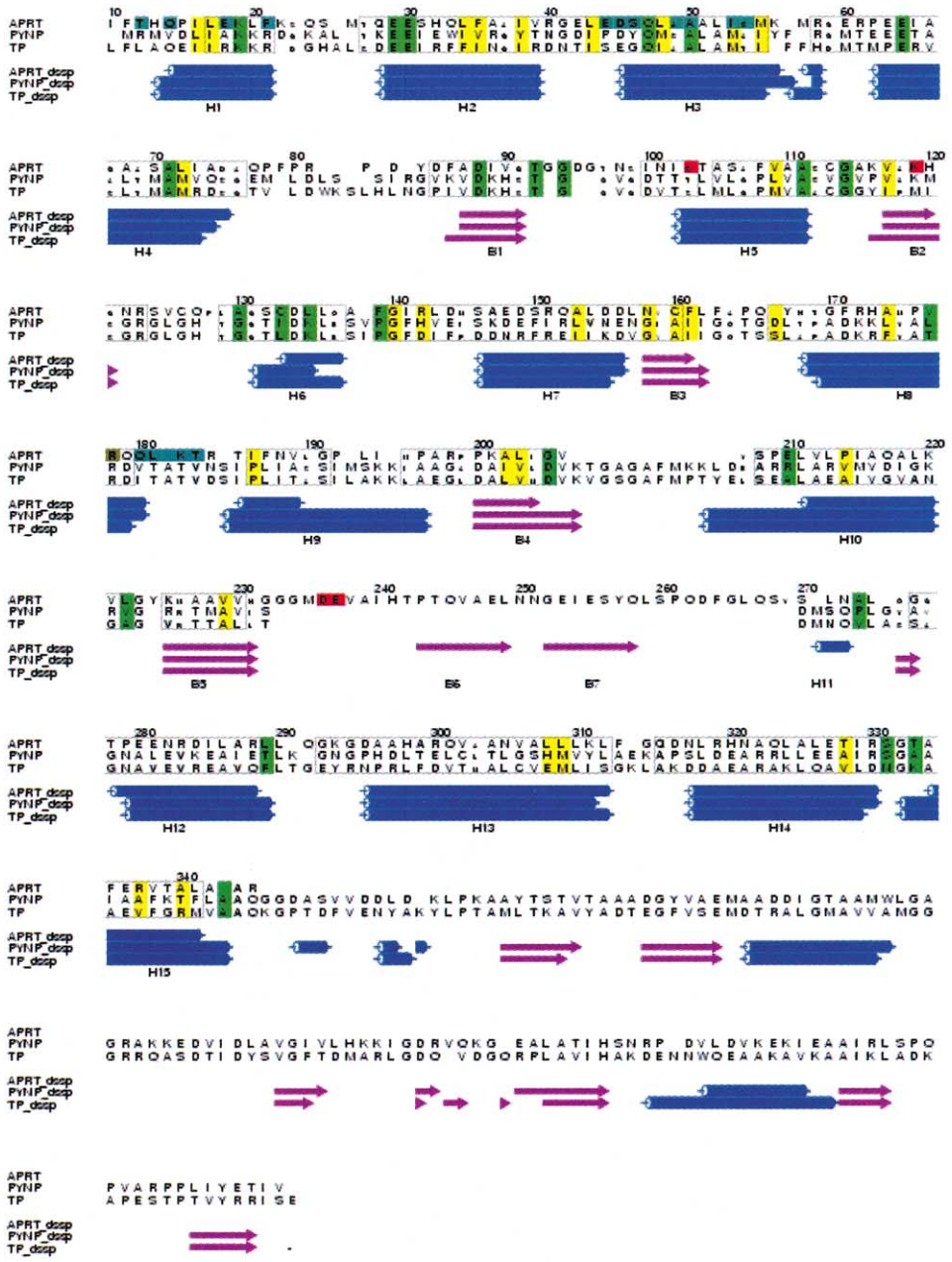

Fig. 1. Sequence alignments of AnPRT, pyrimidine nucleoside phosphorylase and thymidine phosphorylase calculated from aligned structures of the respective molecules. Structure alignment was performed with STAMP [26] and the figure was produced by ALSCRIPT [27]. Secondary structures were assigned by DSSP [28]. Numbering is based on the AnPRT sequence. Conserved hydrophobic residues are shaded yellow, conserved non-hydrophobic residues are shaded green, conserved polar residues are in bold font, conserved small residues in small font and conserved structural regions are shown boxed. Residues involved in PPi–Mn^{2+} binding are shaded red, those involved in the dimer interface in light blue and residues putatively involved in anthranilate binding are shaded gold.

monomers constituting eight subdomains. Initial rigid body refinement of the eight subdomains showed a distinct conformational change in one of monomers relative to the other three. Analysis with HINGEFIND [20] and VMD [21] found the α subdomain of this monomer to be rotated by 9° around an axis relative to the three monomers, thereby narrowing the active cleft. Analogous rotations were found in TP and PYNP. The binding of pseudouridine in PYNP was accompanied by a rotation of 21° [7]. With TP, Pugmire et al. observed a rotation of 9°, comparable to that of AnPRT when two different crystal forms without ligand were compared to a structure solved with a bound SO_4^{2-} [9]. In AnPRT this movement can be attributed to crystal packing although the rotation does demonstrate a degree of flexibility between the subdomains, almost certainly required for catalysis.

3.3. MnPPi binding

The active site of AnPRT is located in the cleft between the α subdomain and the α/β subdomain. The site is defined by H8, H9 from the α subdomain, a loop between B1 and H5 (loop I, residues 90–101), a loop between B2 and H6 (loop II, residues 122–130), and a loop between B5 and B6 (loop III, residues 232–242) from the α/β subdomain (Fig. 2A). Crystallized in the presence of its substrates (anthranilate, PRPP and

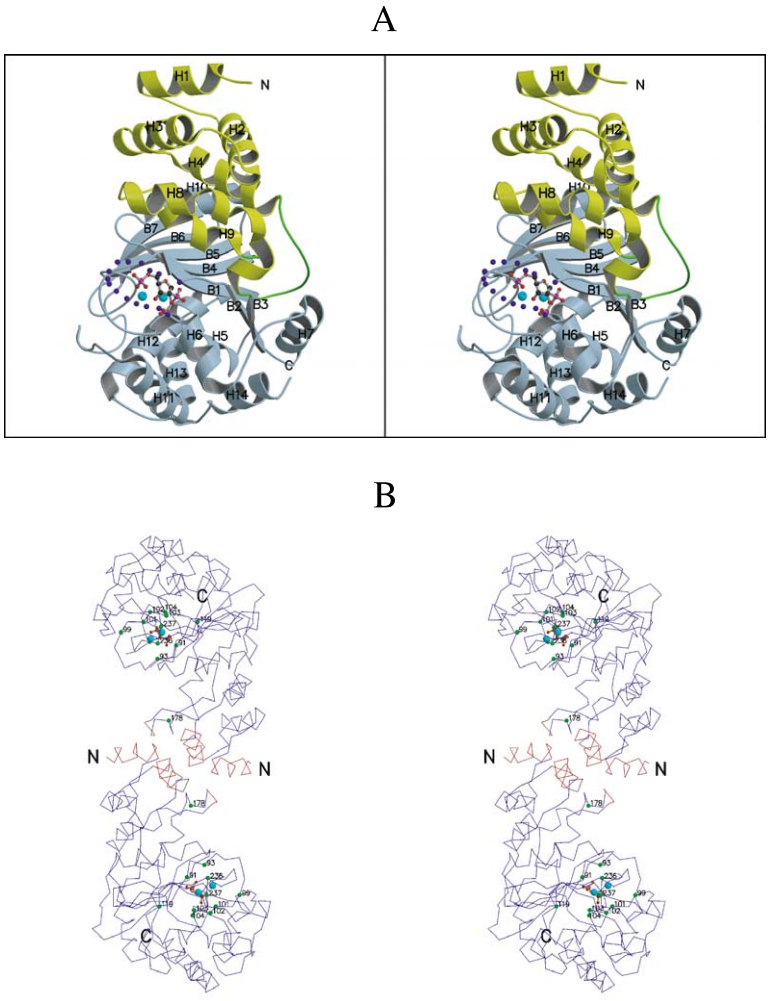

Fig. 2. The structure of AnPRT from *P. carotovorum*. A: Stereo ribbon drawing of a single subunit of AnPRT from *P. carotovorum*. The monomer of AnPRT has two subdomains, α and α/β. The α subdomain in red is a small four-helix bundle, H1–H4, sandwiched next to two additional helices, H8 and H9. The α/β subdomain, blue, consists of eight α-helices (H5–H7, H10–H14) and one mixed sheet, five parallel β-strands (B1–B5) and two anti-parallel β-strands (B6–B7). The observed pyrophosphate with the modeled 5′-ribose phosphate moiety and Mn^{2+} ion are shown as ball-and-stick representation. This figure was produced using MOLSCRIPT [29] and RASTER3D [30]. B: The functional dimeric AnPRT in the asymmetric unit of the MnPPi crystal. The interface region is colored in red. The PPi and Mn^{2+} ions are shown as a ball-and-stick representation. Residues involved in MnPPi and anthranilate binding (G91, G93, S99, N101, I102, S103, T104, K119, R178, D236, E237) are labeled and shown as green balls. R178 is predicted to bind anthranilate as result of the structure comparison with PYNP. This figure was produced using MOLSCRIPT [29] and RASTER3D [30].

Mn^{2+}), the MnPPi crystal showed clear electron density for PPi and two Mn^{2+} ions (MnPPi complex) (Fig. 3A). Weak electron density was also observed near PPi, suggesting the presence of a flexible or low occupancy 5′-ribose phosphate moiety, which was tentatively modeled into the density (Fig. 2A). No comparable electron density was seen in the apoenzyme crystal.

MnPPi is bound between loops I and II (Fig. 3A). It interacts with both loops forming a network of hydrogen bonds with active site residues and water molecules (Fig. 3B,C). PPi forms interactions with MN1, the side chain of Lys119 and the backbone nitrogens of Gly91, Ile102 and Ser103. MN1 is octahedrally coordinated by side chains Ser103, Glu237 and two water molecules, in addition to two oxygen atoms from PPi (Fig. 3B,C). MN2 is also coordinated octahedrally by four water molecules and two acidic side chains, Asp236 and Glu237. Strict conservation of these two electronegative side chains, as well as all the side chains involved in metal and PPi binding, is consistent with the requirement of AnPRTs for divalent cations in catalysis.

3.4. Active site comparison with PYNP

The reactions catalyzed by AnPRT, PYNP, and TP are shown in Scheme 2. The PPi-binding site of AnPRT is in close alignment with the phosphate-binding site of PYNP (Figs. 1 and 4A,B). Superposition of the two structures shows the alignment of the bound PPi and Pi, and many of the active site residues (Figs. 1 and 4B). As shown in Fig. 1, Ser103, Lys119 and Ser132 of AnPRT align with Thr92, Lys108 and Thr120 of PYNP respectively, and these residues interact with PPi and Pi through their polar side chains (Fig. 4B). Gly91 of AnPRT and Ser83 of PYNP are hydrogen bonded with PPi and Pi through the main chain nitrogen (Fig. 3B).

PYNP, crystallized with bound pseudouridine, revealed that Arg168, Ser183, and Lys187 are hydrogen bonded to the substrate [7] (Fig. 4B). In the AnPRT crystal, Arg178, Gly191,

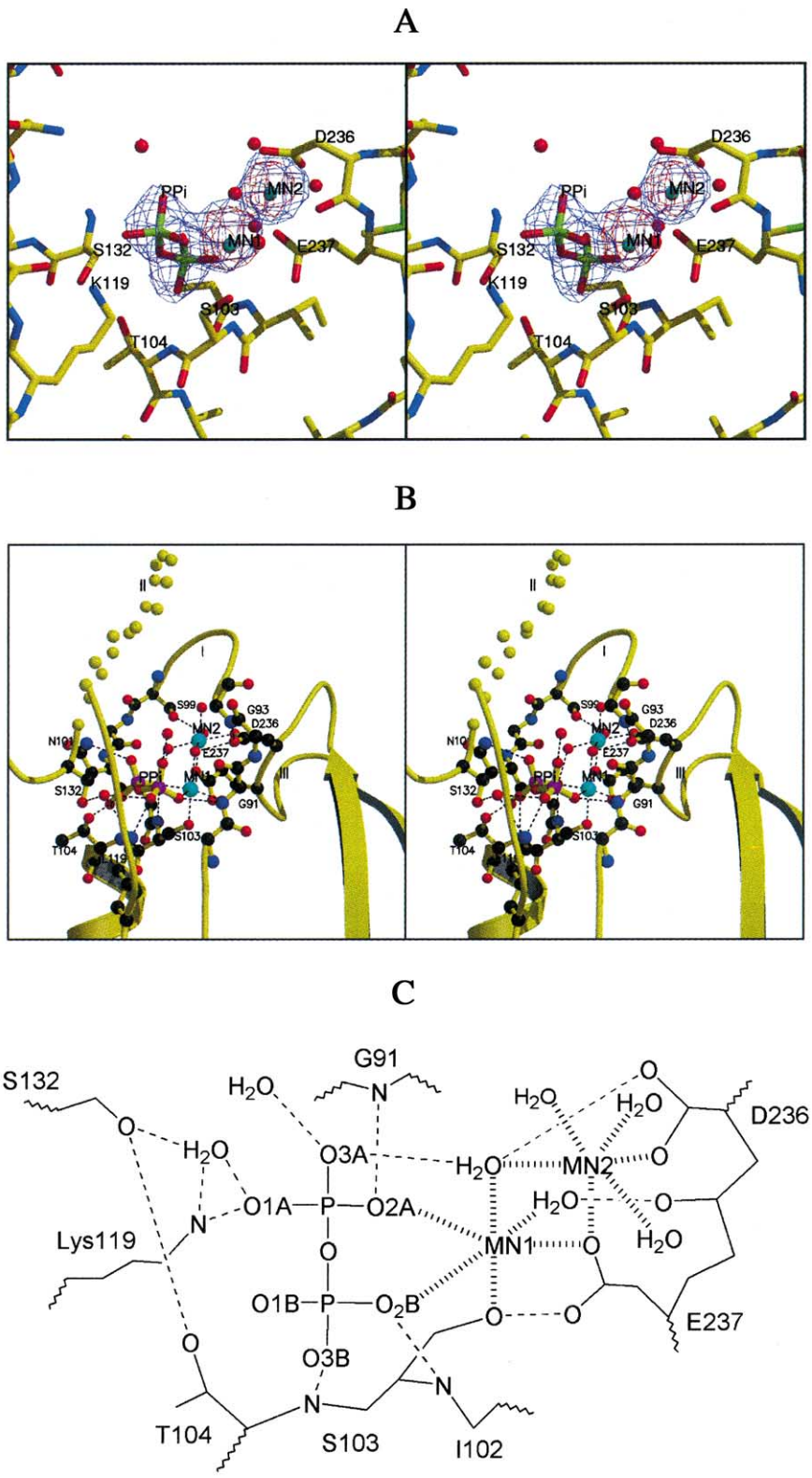

Fig. 3. The active site. A: Stereo diagram of the electron density of PPi and two Mn^{2+} ions at 2.4 Å resolution. Pyrophosphate is colored by atom type (oxygen, red; phosphorous, yellow green). Water molecules and the two Mn^{2+} ions are shown as red and cyan spheres respectively. An anomalous F_o-F_c density map contoured at 5σ (red) shows the electron density of two metal ions. A F_o-F_c omit map contoured at 3σ (violet) shows the density cluster for Mn^{2+}–PPi complex. This figure was produced using Xtalview [16] and RASTER3D [30]. B: The active site of AnPRT showing two octahedrally coordinated Mn^{2+} ions and PPi. Observed contacts are shown in dotted lines. There are three loops in the active site, I, II and III. PPi is firmly bound between active site loops I and III and interacts with both loops by hydrogen bonding to MN1 (cyan), the side chain of Lys119, and the back bone nitrogens of Gly91, Ile102, Ser103 (Fig. 4A,B). Two Mn^{2+} ions are octahedrally coordinated by side chains of Ser103, Asp236, Glu37, water molecules, and PPi. MN1 binds directly to PPi. This figure was produced using MOLSCRIPT [29] and RASTER3D [30]. C: Non-covalent interactions between the enzyme, PPi and Mn^{2+} ions. This figure was produced using CHEMDRAW (CambridgeSoft, Cambridge, MA, USA).

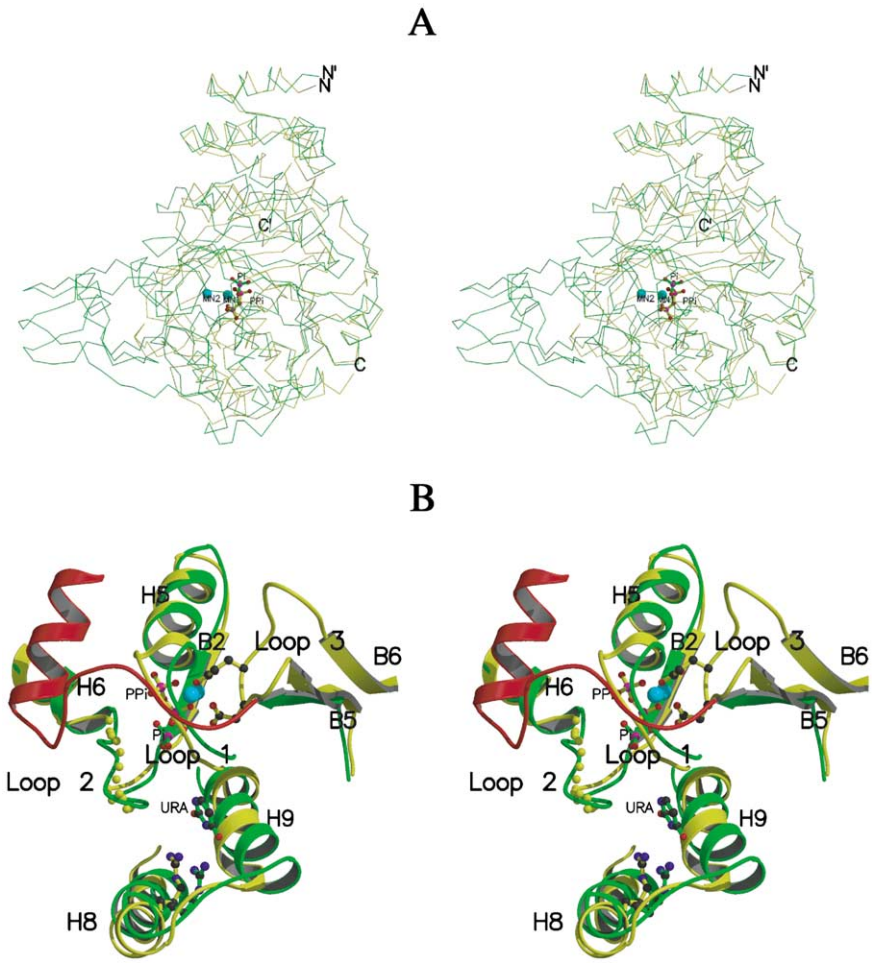

Fig. 4. Structure comparison of AnPRT and PYNP. A: Superposition of AnPRT and PYNP. The stereo view of the AnPRT (yellow) superimposed on the *Bacillus stearothermophilus* PYNP structure (green). The bound pyrophosphate (labeled PPi) of AnPRT (yellow) and the bound phosphate (labeled Pi) of PYNP (green) are shown. The structures are very similar and 230 Cα atoms can be superimposed with an overall rmsd of 2.0 Å. The largest difference is the additional domain missing in AnPRT. This contains seven β-strands forming two anti-parallel β-sheets with three extra helices sandwiched in the middle at the carboxyl terminus. B: Stereo diagram of overlapped active sites of AnPRT and PYNP. The active site of AnPRT is shown in yellow and the active site of PYNP is shown in blue and red. The bound PPi of AnPRT (yellow) aligns closely with the bound Pi of PYNP (green). Active sites of both enzymes are homologous except for a region labeled as loop III. In AnPRT, two acidic residues (yellow) crucial for coordinating two Mn^{2+} ions are on loop III formed between B5 and B6. In PYNP, B5 connected to the additional domain (red). The uracil moiety of pseudouridine (labeled URA, green) bound to PYNP between H8 and H9 interacts with Arg168 (green) and this aligns with Arg178 (yellow) of AnPRT. In AnPRT, Arg178 may interact with its substrate, anthranilate. The dotted spheres (shown in yellow) indicate the disordered loop 2 of AnPRT. This figure was produced using MOLSCRIPT [29] and RASTER3D [30].

and Ile194 are seen to occupy positions homologous to the three PYNP residues (Figs. 1 and 4B). The distance between the structurally conserved Arg168 side chain of PYNP and phosphate is comparable to that of AnPRT's Arg178 side chain to PPi (13.4 Å), suggesting that Arg178 is a major determinant of anthranilate binding (it is to be noted that these residues are in the α subdomain).

Unlike AnPRT, PYNP and TP have no catalytic metal ions [8,9]. Metal binding in AnPRT can be attributed to the inclusion of loop III (residues 232–242) relative to PYNP and TP (Figs. 1, 3B and 4B). This loop contains two acidic residues, Asp236 and Glu237, crucial to the binding of two Mn^{2+} ions (Figs. 3A,B and 4A,B).

3.5. AnPRT and tryptophan biosynthesis

The biosynthesis of L-tryptophan is outlined in Scheme 2. The enzymes catalyzing the reactions that convert chorismate to tryptophan are composed of seven domains designated after their cognate genes. The seven domains exhibit different aggregation patterns in microorganisms and plants (the amino acid is a dietary requirement in animals), but the reactions catalyzed by the domains are everywhere invariant [5].

With respect to the relation between AnPRT and TP, Mushegian and Koonin, in exploring amino acid sequences of enzymes that catalyze hydrolysis or phosphorolysis of the *N*-glycosidic bond in nucleosides and phosphoribosyltransferases, defined two new families, each containing bacterial and eukaryotic proteins [24]. Analysis of the *Escherichia coli* TP and deduced common motifs from TP and AnPRT led to the 'unexpected' inclusion of the enzymes in a single family and suggest that they evolved from a common ancestor. The structural homology observed here between AnPRT and TP lends evidence to their proposal.

The structure solution of AnPRT completes the pathway

enzyme structures. Some preliminary conclusions can be drawn as to their mutual evolutionary relationships. The domains TrpA, TrpC, and TrpF are $(\alpha/\beta)_8$ barrel, are of approximately the same size, denature by a common mechanism, and activate single, closely related molecules. It is, therefore, reasonable to ascribe their origin to gene duplication and divergence. A definitive example of convergence in the pathway is provided by anthranilate synthase, $(TrpE)_2(TrpG)_2$ (Scheme 1). TrpE by itself can utilize NH_3 in the conversion of chorismate to anthranilate. Since it cannot use NH_4^+ ($pK_a = 9.25$) its reaction velocity is sharply curtailed at ordinary pH. The addition of glutamine amidotransferase (GAT) to the pathway circumvents this restriction. Glutamine activation is provided by GAT for many enzymes. In the Bacilli it is identically a component of both *ortho*- and *para*-amino benzoic acid synthases and is an obvious import into the tryptophan pathway. A similar argument pertains to the entirely different structures of TrpA and TrpB, the components of tryptophan synthase. AnPRT is more difficult to assess. Its fold, common to the nucleoside phosphorylases TP and PYNP, is novel with respect to known PRTs. Whether it has arisen through a convergence of domains each activating PRPP and anthranilate, or whether it is a product of a single gene evolving into a two-substrate enzyme remains to be resolved. In summary, the pathway enzymes display five structural folds, one novel (TrpE) [22,23], and the others previously known but each unrelated to the other. It is clear that, as has been shown for the protein ensemble responsible for glycolysis [25], a combination of convergence, and gene duplication and divergence have been the generating forces of L-tryptophan biosynthesis.

Acknowledgements: We thank Charles Yanofsky for his constant support and criticism and Mark Miller, Seungil Han, Benjamin Boe, David Braun and Nick Nguyen for advice and excellent technical assistance. This study was supported by NIH-National Cancer Institutes National Research Service Award T32 CA09532 to C.K. Additional computational support has been provided by the W.M. Keck Foundation.

References

[1] Smith, J.L. (1999) Nat. Struct. Biol. 6, 502–504.
[2] Schumacher, M.A., Carter, D., Ross, D.S., Ullman, B. and Brennan, R.G. (1996) Nat. Struct. Biol. 3, 881–887.
[3] Eads, J.C., Ozturk, D., Wexler, T.B., Grubmeyer, C. and Sacchettini, J.C. (1997) Structure (London) 5, 47–58.
[4] Sharma, V., Grubmeyer, C. and Sacchettini, J.C. (1998) Structure 6, 1587–1599.
[5] Yanofsky, C., Miles, E.W., Bauerle, R. and Kirschner, K. (1999) Encycl. Mol. Biol. 4, 2676–2687.
[6] Largen, M., Mills, S.E., Rowe, J. and Yanofsky, C. (1978) J. Biol. Chem. 253, 409–412.
[7] Pugmire, M.J. and Ealick, S.E. (1998) Structure 15, 1467–1479.
[8] Walter, M.R., Cook, W.J., Cole, L.B., Short, S.A., Koszalka, G.W., Krenitsky, T.A. and Ealick, S.E. (1990) J. Biol. Chem. 256, 14016–14022.
[9] Pugmire, M.J., Cook, W.J., Jasanoff, J., Walter, M.R. and Ealick, S.E. (1998) J. Mol. Biol. 281, 285–299.
[10] Paluh, J.L. and Clayton, D.A. (1996) Yeast 12, 1393–1405.
[11] Otwinowski, Z. and Minor, W. (1997) Methods Enzymol. 276, 307–326.
[12] Sheldrick, G.M. (1997) Methods Enzymol. 276, 628–641.
[13] CCP (1994) Acta Crystallogr. D50, 760–763.
[14] Spraggon, G. (1999) Acta Crystallogr. D55, 458–463.
[15] Cowtan, K. (1994) Int. CCP4/ESF-EACBM Newslett. Protein Crystallogr. 31, 34.
[16] McRee, D.E. (1999) J. Struct. Biol. 125, 156–165.
[17] Brünger, A.T. et al. (1998) Acta Crystallogr. D54, 905–921.
[18] Perrakis, A., Sixma, T.K., Wilson, K.S. and Lamzin, V.S. (1997) Acta Crystallogr. D53, 448–455.
[19] Holm, L. and Sander, C. (1998) Nucleic Acids Res. 26, 316–319.
[20] Wriggers, W. and Schulten, K. (1997) Proteins 29, 1–14.
[21] Humphrey, W., Dalke, A. and Schulten, K. (1996) J. Mol. Graph. 14, 33–38.
[22] Knochel, T., Ivens, A., Hester, G., Gonzalez, A., Bauerle, R., Wilmanns, M., Kirschner, K. and Jansonius, J.N. (1999) Proc. Natl. Acad. Sci. USA 96, 9479–9484.
[23] Spraggon, G., Kim, C., Nguyen-Huu, X., Yee, M.C., Yanofsky, C. and Mills, S.E. (2001) Proc. Natl. Acad. Sci. USA 98, 6021–6026.
[24] Mushegian, A.R. and Koonin, E.V. (1994) Protein Sci. 3, 1081–1088.
[25] Fothergill-Gilmore, L.A. (1987) Biochem. Soc. Trans. 15, 993–995.
[26] Russell, R.B. and Barton, G.J. (1993) J. Mol. Biol. 234, 951–957.
[27] Barton, G.J. (1993) Protein Eng. 6, 37–40.
[28] Kabsch, W. and Sander, C. (1983) Biopolymers 22, 2577–2637.
[29] Kraulis, P.J. (1991) J. Appl. Crystallogr. 24, 946–950.
[30] Merritt, E.A. and Bacon, D.J. (1997) Methods Enzymol. 277, 505–524.